

# Mass-producible and efficient optical antennas with CMOS-fabricated nanometer-scale gap

Tae Joon Seok, Arash Jamshidi, Michael Eggleston, and Ming C. Wu\*

Department of Electrical Engineering and Computer Sciences, University of California, Berkeley, CA 94720, USA  
wu@eecs.berkeley.edu

**Abstract:** Optical antennas have been widely used for sensitive photodetection, efficient light emission, high resolution imaging, and biochemical sensing because of their ability to capture and focus light energy beyond the diffraction limit. However, widespread application of optical antennas has been limited due to lack of appropriate methods for uniform and large area fabrication of antennas as well as difficulty in achieving an efficient design with small mode volume (gap spacing < 10nm). Here, we present a novel optical antenna design, arch-dipole antenna, with optimal radiation efficiency and small mode volume, 5 nm gap spacing, fabricated by CMOS-compatible deep-UV spacer lithography. We demonstrate strong surface-enhanced Raman spectroscopy (SERS) signal with an enhancement factor exceeding  $10^8$  from the arch-dipole antenna array, which is two orders of magnitude stronger than that from the standard dipole antenna array fabricated by e-beam lithography. Since the antenna gap spacing, the critical dimension of the antenna, can be defined by deep-UV lithography, efficient optical antenna arrays with nanometer-scale gap can be mass-produced using current CMOS technology.

©2013 Optical Society of America

**OCIS codes:** (220.0220) Optical design and fabrication; (240.6695) Surface-enhanced Raman scattering; (350.4238) Nanophotonics and photonic crystals.

---

## References and links

1. K. B. Crozier, A. Sundaramurthy, G. S. Kino, and C. F. Quate, "Optical antennas: Resonators for local field enhancement," *J. Appl. Phys.* **94**(7), 4632 (2003).
2. P. Mühlischlegel, H.-J. Eisler, O. J. F. Martin, B. Hecht, and D. W. Pohl, "Resonant optical antennas," *Science* **308**(5728), 1607–1609 (2005).
3. L. Novotny and N. van Hulst, "Antennas for light," *Nat. Photonics* **5**(2), 83–90 (2011).
4. V. Giannini, A. I. Fernández-Domínguez, S. C. Heck, and S. A. Maier, "Plasmonic nanoantennas: fundamentals and their use in controlling the radiative properties of nanoemitters," *Chem. Rev.* **111**(6), 3888–3912 (2011).
5. L. Tang, S. E. Kocabas, S. Latif, A. K. Okyay, D.-S. Ly-Gagnon, K. C. Saraswat, and D. A. B. Miller, "Nanometre-scale germanium photodetector enhanced by a near-infrared dipole antenna," *Nat. Photonics* **2**(4), 226–229 (2008).
6. P. Fan, K. C. Y. Huang, L. Cao, and M. L. Brongersma, "Redesigning photodetector electrodes as an optical antenna," *Nano Lett.* **13**(2), 392–396 (2013).
7. A. Kinkhabwala, Z. Yu, S. Fan, Y. Avlasevich, K. Mullen, and W. E. Moerner, "Large single-molecule fluorescence enhancements produced by a bowtie nanoantenna," *Nat. Photonics* **3**(11), 654–657 (2009).
8. K. J. Russell, T.-L. Liu, S. Cui, and E. L. Hu, "Large spontaneous emission enhancement in plasmonic nanocavities," *Nat. Photonics* **6**(7), 459–462 (2012).
9. M. P. Busson, B. Rolly, B. Stout, N. Bonod, and S. Bidault, "Accelerated single photon emission from dye molecule-driven nanoantennas assembled on DNA," *Nat Commun* **3**, 962 (2012).
10. K. C. Y. Huang, M.-K. Seo, Y. Huo, T. Sarmiento, J. S. Harris, and M. L. Brongersma, "Antenna electrodes for controlling electroluminescence," *Nat Commun* **3**, 1005 (2012).
11. C. Höppener and L. Novotny, "Antenna-based optical imaging of single Ca<sup>2+</sup> transmembrane proteins in liquids," *Nano Lett.* **8**(2), 642–646 (2008).
12. T. S. van Zanten, M. J. Lopez-Bosque, and M. F. Garcia-Parajo, "Imaging individual proteins and nanodomains on intact cell membranes with a probe-based optical antenna," *Small* **6**(2), 270–275 (2010).
13. W. A. Challener, C. Peng, A. V. Itagi, D. Karns, W. Peng, Y. Peng, X. Yang, X. Zhu, N. J. Gokemeijer, Y.-T. Hsia, G. Ju, R. E. Rottmayer, M. A. Seigler, and E. C. Gage, "Heat-assisted magnetic recording by a near-field transducer with efficient optical energy transfer," *Nat. Photonics* **3**(4), 220–224 (2009).

14. D. P. Fromm, A. Sundaramurthy, A. Kinkhabwala, P. J. Schuck, G. S. Kino, and W. E. Moerner, "Exploring the chemical enhancement for surface-enhanced Raman scattering with Au bowtie nanoantennas," *J. Chem. Phys.* **124**(6), 061101 (2006).
15. W. Zhu, M. G. Banaee, D. Wang, Y. Chu, and K. B. Crozier, "Lithographically fabricated optical antennas with gaps well below 10 nm," *Small* **7**(13), 1761–1766 (2011).
16. A. Ahmed and R. Gordon, "Single molecule directivity enhanced raman scattering using nanoantennas," *Nano Lett.* **12**(5), 2625–2630 (2012).
17. P. J. Schuck, D. P. Fromm, A. Sundaramurthy, G. S. Kino, and W. E. Moerner, "Improving the mismatch between light and nanoscale objects with gold bowtie nanoantennas," *Phys. Rev. Lett.* **94**(1), 017402 (2005).
18. M. W. Knight, L. Liu, Y. Wang, L. Brown, S. Mukherjee, N. S. King, H. O. Everitt, P. Nordlander, and N. J. Halas, "Aluminum Plasmonic Nanoantennas," *Nano Lett.* **12**(11), 6000–6004 (2012).
19. Y.-K. Choi, T.-J. King, and C. Hu, "A spacer patterning technology for nanoscale CMOS," *IEEE Trans. Electron Devices* **49**(3), 436–441 (2002).
20. Y.-K. Choi, J. Zhu, J. Grunes, J. Bokor, and G. A. Somorjai, "Fabrication of Sub-10-nm silicon nanowire arrays by size reduction lithography," *J. Phys. Chem. B* **107**(15), 3340–3343 (2003).
21. T. J. Seok, A. Jamshidi, M. Kim, S. Dhuey, A. Lakhani, H. Choo, P. J. Schuck, S. Cabrini, A. M. Schwartzberg, J. Bokor, E. Yablonovitch, and M. C. Wu, "Radiation engineering of optical antennas for maximum field enhancement," *Nano Lett.* **11**(7), 2606–2610 (2011).
22. S. A. Maier, "Plasmonic field enhancement and SERS in the effective mode volume picture," *Opt. Express* **14**(5), 1957–1964 (2006).
23. T. Feichtner, O. Selig, M. Kiunke, and B. Hecht, "Evolutionary optimization of optical antennas," *Phys. Rev. Lett.* **109**(12), 127701 (2012).
24. M. Fleischmann, P. J. Hendra, and A. J. McQuillan, "Raman spectra of pyridine adsorbed at a silver electrode," *Chem. Phys. Lett.* **26**(2), 163–166 (1974).
25. D. L. Jeanmaire and R. P. Van Duyne, "Surface raman spectroelectrochemistry: Part I. Heterocyclic, aromatic, and aliphatic amines adsorbed on the anodized silver electrode," *J. Electroanal. Chem. Interfacial Electrochem.* **84**(1), 1–20 (1977).
26. K. Kneipp, Y. Wang, H. Kneipp, L. T. Perelman, I. Itzkan, R. R. Dasari, and M. S. Feld, "Single molecule detection using Surface-Enhanced Raman Scattering (SERS)," *Phys. Rev. Lett.* **78**(9), 1667–1670 (1997).
27. S. Nie and S. R. Emory, "Probing single molecules and single nanoparticles by Surface-Enhanced Raman Scattering," *Science* **275**(5303), 1102–1106 (1997).
28. D.-K. Lim, K.-S. Jeon, H. M. Kim, J.-M. Nam, and Y. D. Suh, "Nanogap-engineerable Raman-active nanodumbbells for single-molecule detection," *Nat. Mater.* **9**(1), 60–67 (2010).
29. D.-K. Lim, K.-S. Jeon, J.-H. Hwang, H. Kim, S. Kwon, Y. D. Suh, and J.-M. Nam, "Highly uniform and reproducible surface-enhanced Raman scattering from DNA-tailorable nanoparticles with 1-nm interior gap," *Nat. Nanotechnol.* **6**(7), 452–460 (2011).
30. Y. Fang, N.-H. Seong, and D. D. Dlott, "Measurement of the distribution of site enhancements in Surface-Enhanced Raman Scattering," *Science* **321**(5887), 388–392 (2008).

---

## 1. Introduction

Optical antennas [1–4] have been widely used for a variety of applications such as sensitive photodetection [5,6], enhanced light emission [7–10], high resolution imaging [11,12], heat-assisted magnetic recording [13], and surface-enhanced Raman spectroscopy (SERS) [14–16] since they can capture and focus propagating electromagnetic energy into sub-diffraction-limited area, and vice versa. The antenna performance of focusing localized optical energy or enhancing the emitter efficiency critically depends on the small (a few nanometers-scale) high field region such as the antenna feed gap [15,17], which can be achieved by focused ion-beam (FIB) and electron beam (e-beam) but with poor uniformity and reproducibility for critical dimensions below 10 nm and limited fabrication area. Recently, aluminum optical antennas have been reported with promising potential as a CMOS-compatible process [18], however, the resolution limit of current CMOS technology is not fine enough to guarantee nanometer-scale gap dimensions. Therefore, designing efficient optical antennas with extremely small mode volumes and large area fabrication capabilities remains a challenging problem for the practical usage of optical antenna applications.

In this paper, we demonstrate a novel optical antenna design, arch-dipole antenna, with 5 nm gap spacing fabricated by CMOS process. In this process, the gap spacing of the arch-dipole antenna is determined by the thickness of a thin dielectric fin using deep-UV spacer lithography [19,20]. Since the fin layer is deposited by atomic layer deposition (ALD), the thickness of the fin can be precisely controlled with sub-nm accuracy and good reproducibility. In this design, the optimum fin height is chosen to control the radiation of the arch-dipole antenna, which enables matched radiation and absorption quality factors for the

maximum field enhancement [21]. As an experimental verification of antenna performance, SERS signal from *trans*-1,2-bis (4-pyridyl) ethylene (BPE) has been measured on the fabricated gold arch-dipole antenna array. The SERS enhancement factor measured from the arch-dipole antenna array is two orders of magnitude greater than that from a typical dipole antenna array fabricated by e-beam lithography.

## 2. Design and simulation

It has been previously shown using coupled mode theory (CMT) that the field enhancement of an optical antenna on resonance can be derived as [21,22]:

$$\frac{|E_{loc}|^2}{|E_i|^2} = \frac{2A_c \lambda_{res}}{\pi} \frac{Q}{Q_{rad}} \frac{Q}{V_{eff}} \quad (1)$$

where  $E_{loc}$  and  $E_i$  are the local field amplitude at the high field region of an optical antenna and the field amplitude of incoming wave.  $A_c$ ,  $V_{eff}$ ,  $Q$ , and  $Q_{rad}$  are the maximum effective aperture, the effective mode volume, the total quality factor and the radiation quality factor of the optical antenna, respectively. From the equation, we can extract two main conditions to achieve the maximum field enhancement of an optical antenna: 1) the matched quality factors ( $Q_{rad} = Q_{abs}$ ) to maximize the quality factors related term,  $Q^2/Q_{rad}$  [21], and 2) the small antenna gap to minimize the effective mode volume,  $V_{eff}$  [15].

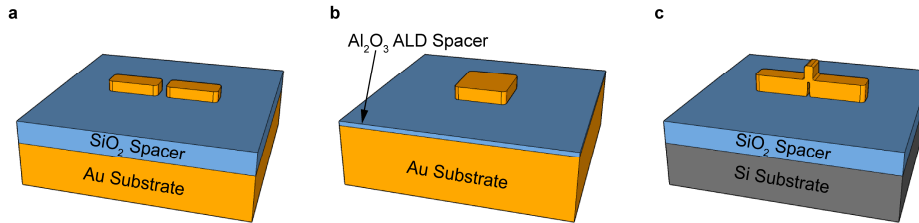


Fig. 1. Schematics of optical antenna designs. (a) Dipole antenna on ground plane for matched quality factors. (b) Patch antenna for sub-10 nm gap spacing. (c) Arch-dipole antenna for matched quality factors and sub-10 nm gap spacing.

Figure 1 shows three different designs of optical antennas to address these conditions. The dipole antenna on dielectric spacer coated ground plane, shown in Fig. 1(a), has been reported to achieve the quality factors matching condition [21]. In this antenna design, the radiation characteristic of optical antennas is controlled by tuning the thickness of the dielectric spacer layer. However, it is challenging to reduce the gap spacing of dipole antennas below 10 nm since optical antennas are typically fabricated by nanofabrication techniques such as e-beam lithography or focused ion beam (FIB) milling, which have poor uniformity and reproducibility below 10 nm dimension. To resolve this fabrication issue, the second design, the optical patch antenna, has been suggested, which can be easily fabricated with uniform sub-10 nm gap [Fig. 1(b)]. Since the dielectric spacer layer between the top nanopatch and the ground plane defines the antenna gap spacing, it can be easily reduced below 5 nm with sub-nm accuracy by atomic layer deposition (ALD). The patch antenna, however, has poor radiation efficiency as we reduce the gap to nanometer scale, which results in a large mismatch between  $Q_{rad}$  and  $Q_{abs}$ . Therefore, the field enhancement stops increasing with shrinking gap spacing as shown in Fig. 2. To overcome the trade-off between radiation efficiency and small gap spacing, we have developed a new antenna design “arch-dipole antenna,” the main subject of this paper. In the arch-dipole antenna, the two arms of a dipole antenna are connected by a tall narrow arch as shown in Fig. 1(c). Similar optical antennas have been reported with numerical simulations for efficient field enhancement [23]. The antenna gap inside the arch can be defined by the thickness of a sacrificial dielectric layer using spacer lithography. The arch-dipole antenna design offers a robust method for uniform

and reproducible fabrication of sub-10 nm gap spacing without the sacrifice of radiation efficiency.

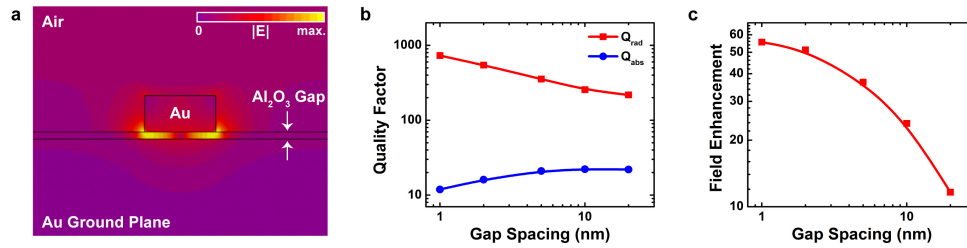


Fig. 2. Numerical simulations of gold patch antenna array. (a) Electric field profile of gold patch antenna. Patch antennas with dimensions of 50 nm square size, 25 nm thickness, and 5 nm  $Al_2O_3$  gap were simulated with periodic boundary condition of 300 nm pitch. (b) Plot of calculated radiation and absorption quality factors as a function of gap spacing. (c) Plot of electric field enhancement as a function of gap spacing. Patch antenna arrays with various gap spacings (1, 2, 5, 10, and 20 nm) were simulated. Due to the growing mismatch between radiation and absorption quality factors, the increasing ratio of the field enhancement is suppressed as the gap is reduced below 2 nm.

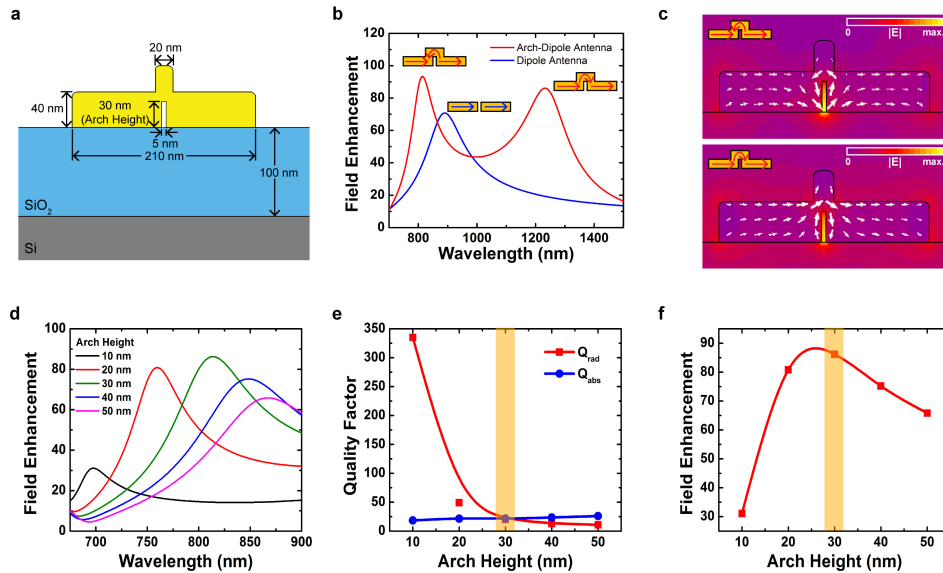


Fig. 3. Numerical simulations of gold arch-dipole antenna array. (a) Schematic of the simulated structure. 210 nm long, 50 nm wide, and 40 nm thick gold arch-dipole antennas with 5 nm gap and 30 nm arch height were simulated. Periodic boundary condition was used to calculate an antenna array with 600 nm pitch. (b) Electric field enhancement of arch-dipole antenna (red curve). Standard dipole antenna with same gap and length was also simulated for comparison (blue curve). Arch-dipole antenna has two modes depending on the current direction in the arch. (c) Electric field magnitude profile of simulated arch-dipole antennas. White arrows in antennas represent the current distribution. (d)-(f) Simulations of arch-dipole antennas with various arch heights. Field enhancement spectra show a maximum from arch-dipole antennas with 30 nm arch height (d). Quality factor (e) and field enhancement (f) were also plotted as a function of arch height. The field enhancement has a maximum peak at the optimum arch height for  $Q$ -matching condition ( $Q_{rad} = Q_{abs}$ ).

To understand the characteristic of the arch-dipole antenna, we have investigated time domain simulations of a gold arch-dipole antenna with 210 nm length, 50 nm width, 40 nm thickness, and 5 nm gap [Fig. 3(a)]. A dipole antenna with same length, width, thickness and gap dimensions has been also simulated for the comparison. The field enhancement plot in Fig. 3(b) shows that the arch-dipole antenna has two resonant modes dependent on the current

direction in the arch whereas a normal dipole antenna has a single fundamental mode. The field enhancements of two arch-dipole antenna modes are higher than the normal dipole antenna with the same gap spacing since the  $Q$  matching condition is achieved for the arch-dipole antenna by tuning the arch height. Here, we have selected the higher frequency mode (the arch current in the opposite direction relative to the antenna arm current) because the antenna dimensions are easier to fabricate (longer length for the desired resonance).

The arch-dipole antennas with various arch heights have been simulated to estimate the effect of the arch height dimension for the antenna characteristics. Figure 3(d) shows the field enhancement of arch-dipole antenna with various arch heights. Radiation and absorption quality factors ( $Q_{rad}$  and  $Q_{abs}$ ) were also calculated from the simulations and it turned out that the radiation of the antenna improves as the arch height increases as shown in Fig. 3(e). As a result, the field enhancement is maximized when  $Q_{rad}$  is matched to  $Q_{abs}$  at the arch height of 30 nm [Fig. 3(f)].

### 3. Fabrication and experimental results

For the experimental demonstration, we have used deep-UV spacer lithography to define the gap spacing and the arch height of the antenna, as shown in Fig. 4(a).

First, an amorphous Si (a-Si) layer is deposited on top of a 100 nm thick thermal oxide layer coated Si wafer. The thickness of a-Si layer determines the dimension of the arch height and the thickness of 30 nm for a-Si layer is chosen since our simulation confirms the  $Q$ -matching condition is achieved at this thickness. After patterning the a-Si layer into 600 nm pitch grating ridges by deep UV lithography and reactive ion etching (RIE), a 5 nm thick aluminum oxide ( $Al_2O_3$ ) layer is conformally deposited by atomic layer deposition (ALD), which enables the thickness control with sub-nm accuracy. The horizontal part of the  $Al_2O_3$  layer is etched away by RIE etching, leaving only  $Al_2O_3$  film on the sidewalls of a-Si ridges. After selective etching of a-Si ridges using  $XeF_2$ , the  $Al_2O_3$  films become free-standing fins, which have dimensions of 5 nm width and 30 nm height [Fig. 4(b)]. A 40 nm thick gold of rectangular array pattern is deposited on the fin to form arch-dipole antennas with uniform arch gap and height [Fig. 4(c)]. Finally, the  $Al_2O_3$  fins are removed to open gaps of arch-dipole antennas by hot phosphoric acid [Fig. 4(d)]. Since the arch gap and height, critical dimensions for the antenna characteristic, are defined by the thicknesses of  $Al_2O_3$  ALD layer and a-Si sacrificial layer, those dimensions can be uniformly and reproducibly demonstrated with high precision dimension control.

We used reflectance measurements to characterize antenna resonances. Figure 5(a) shows the reflectance spectrum from the arch-dipole antenna array with 210 nm length, 50 nm width, 40 nm thickness, and 5 nm gap, which are comparable dimensions to the simulated antenna array. A Si CCD camera is used to measure reflectance for the wavelength range from 500 nm to 950 nm and an InGaAs CCD camera is used for the range from 950 nm to 1500 nm. The reflectance measurement clearly shows two main antenna modes of the arch-dipole antenna around 800 nm and 1300 nm as predicted from the simulation. For the resonance tuning, antenna arrays with various antenna lengths (150, 180, 210, and 240 nm) were fabricated and the resonance shifts of the higher frequency mode are shown in the inset of Fig. 5(a).

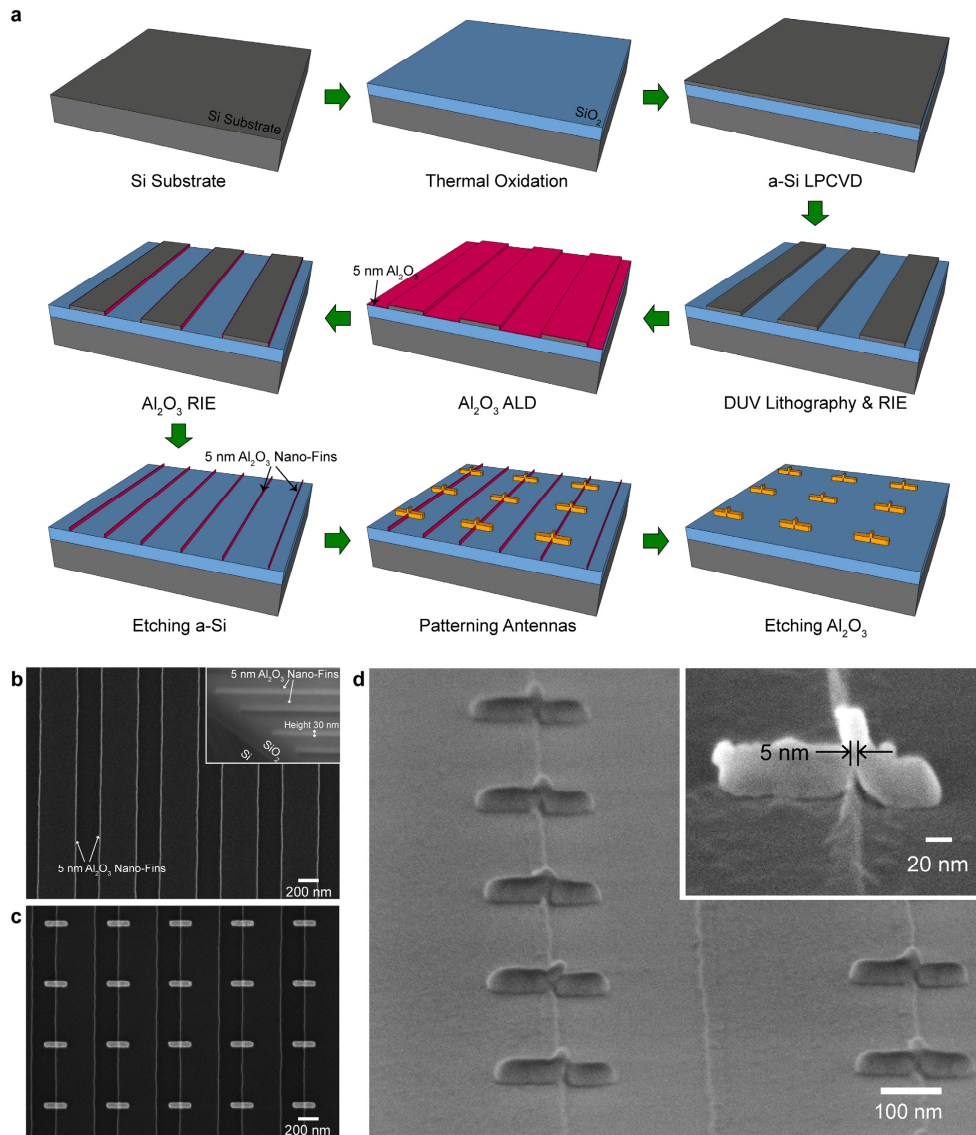


Fig. 4. Fabrication of the arch-dipole antennas. (a) Fabrication process of arch-dipole antenna. (b) SEM image of 5 nm  $\text{Al}_2\text{O}_3$  nano-fins. The inset shows a perspective view of nano-fins. (c) SEM image of arch-dipole antenna array before etching  $\text{Al}_2\text{O}_3$  fins. (d) Perspective view SEM image of arch-dipole antennas after etching  $\text{Al}_2\text{O}_3$  fins. The inset shows the zoomed-in view of a representative single antenna.

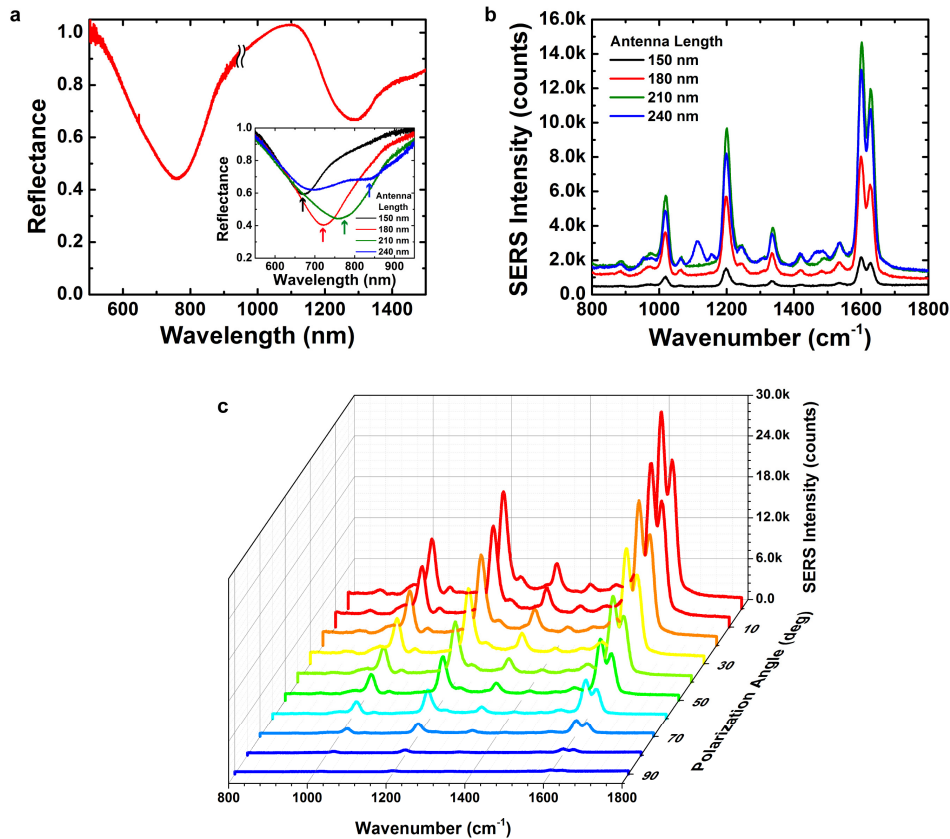


Fig. 5. Reflectance and SERS measurements of gold arch-dipole antenna array. (a) Reflectance measurement of arch-dipole antenna array with 210 nm length, 50 nm width, 40 nm thickness, 5 nm gap and 30 nm arch height. The reflectance spectrum confirms two antenna modes of arch-dipole antenna as expected in simulation. The inset shows the resonance shifts of higher frequency mode with antenna length variations. (b) Measured SERS spectra from *trans*-1,2-bis (4-pyridyl) ethylene (BPE) molecule. The strongest SERS signals were observed from antenna arrays (210 nm and 240 nm long antenna arrays) of which resonances were close to excitation laser wavelength (785 nm) and Stokes shifted wavelength (~870 nm). (c) SERS measurements with various angles of excitation polarization. Strong dependency on antenna resonance and excitation polarization is a clear evidence that SERS signals are resulted from optical antenna.

For the experimental verification of antenna performance, surface-enhanced Raman scattering (SERS) was measured from fabricated optical antenna arrays. SERS has been known as a powerful technique to detect biological and chemical molecule as Raman spectrum provides a unique fingerprint of the target molecule. In order to enhance the sensitivity of SERS, various approaches such as rough surface of metal layer [24,25], metal nanoparticle aggregates [26,27], and DNA-tailored nanoparticle synthesis [28,29] have been previously studied. Though these methods could promise high SERS enhancement enabling single molecule detection, the controllability of hot spot locations still remains challenging [30]. To address this challenge, top-down fabrication of optical antennas has been used to generate SERS hotspots with the engineered spatial arrangement and the reproducible enhancement factors [14–16].

For SERS measurements, *trans*-1,2-bis (4-pyridyl) ethylene (BPE) was used as the target molecule. Fabricated antenna arrays were immersed in a 6 mM solution of BPE in methanol for 2 hours. After 2 hours incubation, the samples were rinsed using methanol, and then blow-dried with nitrogen gun. The excitation from 785 nm laser was focused on the antenna array

using a 10x objective and the Raman signal was collected through the same objective lens for 0.1 sec for SERS measurement. Figure 5(b) shows the measured SERS spectra from antenna arrays with various antenna lengths. The antenna arrays with short lengths (150 nm and 180 nm) exhibit weak SERS signals since the resonance wavelengths are far from the excitation laser wavelength. The measured SERS signals increase as the resonances of the antenna arrays move close to the excitation wavelength and Stokes shifted wavelength with longer antenna lengths (210 nm and 240 nm). The effect of the excitation polarization was also investigated with various angles of polarized excitation [Fig. 5(c)]. The strongest SERS signal was observed when the polarization of the excitation is parallel to the antenna arms and the signal decreases as the excitation polarization approaches to the perpendicular to the antenna arm axis. The strong dependences on the antenna length and the excitation polarization confirm that the SERS signals are resulted from the optical antennas.

To compare the enhancement of SERS signals for different antenna designs, we also measured SERS from dipole antenna arrays and patch antenna arrays. The gold dipole antenna arrays have been fabricated on the dielectric spacer layer ( $\text{SiO}_2$ ) coated gold ground plane by typical e-beam lithography and have the gap spacing of 15 nm, which is practically reproducible. The  $\text{SiO}_2$  spacer thickness is chosen to be 100 nm which has the maximum enhancement by  $Q$  matching condition [21]. For the gold patch antenna arrays, smaller gaps such as 1 nm have been demonstrated, however, the poor radiation efficiency and the mismatch between the radiation  $Q$  and the absorption  $Q$  suppress the efficiency of the antenna. The optimal SERS spectra from dipole antenna, patch antenna, and arch-dipole antenna arrays are shown in Fig. 6(a). The average and hotspot enhancement factors at the 1200  $\text{cm}^{-1}$  Raman shift peak were calculated assuming monolayer coating of BPE molecules on the total antenna surfaces and sidewall surfaces at the antenna gap, respectively [Fig. 6(b)]. The arch-dipole antenna has above  $10^8$  SERS enhancement factor for the average calculation and  $10^9$  enhancement factor for the hotspot calculation, which is about two orders of magnitude stronger than dipole antenna, and an order of magnitude stronger than the patch antenna.

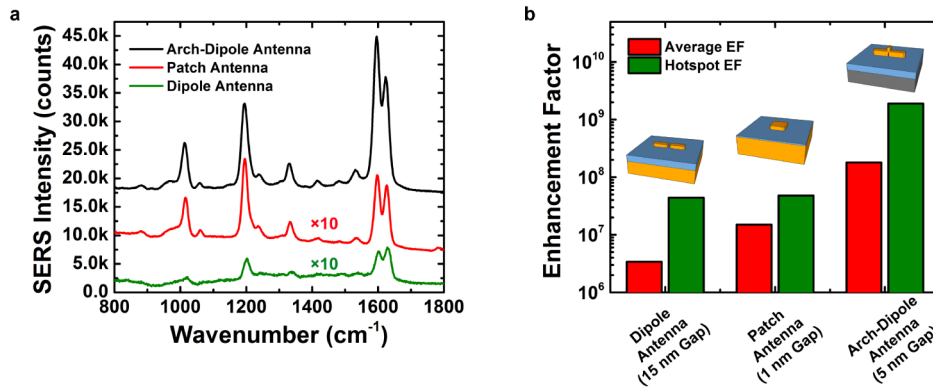


Fig. 6. Comparison of measured SERS signals and calculated SERS enhancement factors from dipole antenna, patch antenna, and arch-dipole antenna. (a) SERS signals measured from different optical antenna designs. SERS spectra from dipole antenna array and patch antenna array were magnified by a factor of 10 for clarity. (b) Calculated SERS enhancement factors. Average enhancement factors were calculated assuming monolayer coating of BPE molecules on entire antenna surface. Hotspot enhancement factors were calculated from molecules coated on the sidewalls of antenna gap.

#### 4. Conclusion

In conclusion, we introduce a new antenna design, arch-dipole antenna, which can be reproducibly fabricated with uniform gap spacing below 10 nm. Since the critical dimensions of arch-dipole antennas can be precisely controlled with sub-nm accuracy, the arch-dipole

antenna can be demonstrated with small gap (sub-10 nm) and  $Q$  matching condition. SERS experiment comparisons with dipole antenna and the patch antenna has been also investigated using identical conditions such as the target molecule, the coating method for molecules, the measurement setup and the enhancement calculation. The dipole antenna design can achieve the  $Q$  matching condition by optimizing the spacer thickness between the antenna array and the ground plane, however, reducing the gap spacing below 10 nm is challenging by typical nanofabrication techniques such as e-beam lithography and focused ion beam milling. On other hand, the patch antenna can be easily implemented with extremely small gaps, however, the poor radiation efficiency and the mismatched  $Q$  factors degrade the antenna performance. The arch-dipole antenna offers an efficient way to achieve small mode volume and  $Q$  matching condition without trade-off between them. As a result, the SERS enhancement factor from the arch-dipole antenna has been observed to be up to two orders of magnitude stronger than those from the other antenna designs. Since the gap spacing, which is the most critical dimension for the enhancement, can be defined by deep UV spacer lithography, wafer-scale SERS substrate with nanometer-scale gap optical antennas can be mass-produced in current CMOS foundries.

### **Acknowledgment**

This work was supported in part by DARPA SERS S&T Fundamentals No. FA9550-08-1-0257. This work was also funded by the Center for Energy Efficient Electronics Science through a grant from the National Science Foundation (NSF Award ECCS-0939514).